PHYSICAL REVIEW A VOLUME 25, NUMBER 1 JANUARY 1982

Electron ionization of some low-Z ions in the plane-wave Born approximation

E. J. McGuire
Sandia National Laboratories, Albuquerque, New Mexico 87185
(Received 22 June 1981)

Explicit plane-wave Born-approximation (PWBA) calculations are presented for electron ionization of ions of carbon, nitrogen, oxygen, and fluorine. Calculations of inner-shell excitation followed by autoionization are included. For ions of carbon, nitrogen, and oxygen, agreement with Coulomb-Born calculations is better than 15% except near threshold; agreement with experiment is better than 25% except near threshold, and except for the Be-like ions N^{3+} and O^{4+}. For fluorine ions, explicit PWBA calculations are presented. These cross sections are as much as 40% higher than results obtained via a scaling procedure. A reexamination of the scaling mechanics indicates an inherent 15% error at high incident electron energy. An attempt is made to correct the error near the cross-section maximum by using an integral over the optical limit of the generalized oscillator strength and its momentum-transfer derivative. The correction is only partially successful because of significant changes in the shape of the generalized oscillator strength with increasing degree of ionization, near squared momentum transfer equal to ionization energy, and secondary electron energy much less than ionization energy.

I. INTRODUCTION

The magnetic fusion program has generated a substantial body of experimental data and theoretical calculations on the cross section for electron ionization of low-Z positive ions. The theoretical approaches include the semiempirical formula of Lotz,[1] the exchange classical impact parameter (ECIP) method,[2] scaled hydrogenic calculations,[3] the Coulomb-Born approach of Moores[4] and Stingl,[5] and the distorted-wave approach of Younger.[6] Earlier, I presented[7] results in scaled form for neutral atom subshell electron ionization cross sections in the plane-wave Born approximation (PWBA). These scaled subshell cross sections were used to compute the cross section for electron ionization of positive ions. For ions with filled and almost filled shells, i.e., Ne^{1+}, Na^{1+}, and Mg^{2+}, the calculations based on scaled cross sections were in excellent agreement with experiment. For ions with half-filled or less than half-filled outer shells, the calculations using scaled cross sections were substantially (as much as a factor of 1.6) lower than the measurements. A tentative conclusion was that the PWBA was inapplicable to these ions.

This tentative conclusion is incorrect. The fault lies in the use of the scaled cross sections. In Sec. II it is shown that numerical PWBA calculations are in excellent agreement with the Coulomb-Born results of Moores[4,8] for ions of carbon, nitrogen, and oxygen.

These calculations were motivated by the needs of the light-ion-beam inertial confinement fusion program, i.e., calculations of the range and stopping power of light ions in high-Z target atoms and ions. Our approach is the generalized oscillator strength (GOS) formulation of the PWBA. If cross-section calculations based on these GOS could not reproduce measured results for electron-light ion systems, they would be of dubious value for light-ion–heavy-ion systems. The excellent agreement with the Coulomb-Born results shown in Sec. II suggests that except near threshold, in ionization calculations it is a minor point whether the projectile sees a neutral or a charged target.

As part of the data base for the light-ion–heavy-ion calculations, GOS for inner- and outer-shell excitation of the light ions were obtained. The inner-shell ($1s$ and $2s$) excitation cross sections were used to determine the contribution of autoionizing levels to the measured ionization cross section.

My first indication that the scaled cross sections required correction came in a study of the proton stopping power of gold ions.[9] A correction to the scaled cross sections, applicable to ions, was obtained in terms of an integral over the difference in optical oscillator strengths of the parent atom and a pseudoatom with the same subshell ionization en-

ergy as the ion. The applicability of this correction to electron ionization of positive ions is examined in Sec. III.

II. NUMERICAL CALCULATIONS

The subshell electron ionization cross section is given by

$$\sigma_{nl}=\frac{4\pi a_0^2}{E_0}\int_0^{\epsilon_{\max}}\frac{d\epsilon}{(\epsilon+E_{nl})}\times\int_{K^2_{\min}}^{K^2_{\max}}\frac{dK^2}{K^2}\sum_{l'=0}^{\infty}\frac{df_{nl}}{d\epsilon}(\epsilon,K^2,l)\ ,$$

where[10]

$$\epsilon_{\max}=\tfrac{1}{2}(E_0-E_{nl})\ ,$$

and

$$K^2_{\substack{\max\\ \min}}=(\sqrt{E_0}\pm\sqrt{E_0-\epsilon-E_{nl}})^2\ . \tag{1}$$

For excitation $\epsilon+E_{nl}$ is replaced by $(E_{n'l'}-E_{nl})$, the integral over ϵ is omitted and the summation is restricted to a single l' value. Details of the GOS calculational procedure are presented elsewhere.[11] The one-electron orbitals were found as solutions to the Schrödinger equation with a central potential generated by a piecewise continuous straight-line approximation to the quantity $[-rV(r)]$ of Herman and Skillman.[12] For the ions considered here six straight lines were used, and for bound orbitals the model eigenvalues agreed with those of Herman and Skillman[12] to 1% or better. With the piecewise continuous approximation the Schrödinger equation is exactly solvable in terms of Whittaker functions, permitting the relatively rapid generation of continuum orbitals. The final-state one-electron orbitals in the excitation calculations were 2*s*-5*s*, 2*p*-5*p*, and 3*d*-5*d*.

In determining the contribution of autoionization to the measured ionization cross section, all final states of the form $1s^1 2s^m 2p^n n'l'$ were assumed to autoionize rapidly. Terms of the form $1s^1 2s^1 nl\ ^4L$ are known to be long lived. However, in the PWBA, spin selection rules forbid the excitation of these terms from a $1s^2 2s\ ^2S$ ground state. Excitation of the 2*s* subshell followed by autoionization was considered only for terms above the first ionization potential as found in Moore's tables.[13] All such terms arising from the configurations $1s^2 2s^1 2p^n n'l'$, with $n\geq 2$, were treated as rapidly autoionizing. From the term $1s^2 2s^2 2p^1\ ^2P$, the Born approximation allows excitation to $1s^2 2s^1 2p^1 n'l'\ ^2L$, where $L=1$ for $l'=0$ and $L=l'\pm 1$, and $L=l'$ for $l'\geq 1$. Parity conservation for Auger decay to ($1s^2 2s^2\ ^1S$ + continuum electron) restricts the continuum electron value (l_c) to $l_c=l'\pm 1$. Thus the final state (^1S core plus continuum electron) is $^2l'\pm 1$. Since the electrostatic interaction conserves both L and S, only the initial $^2l'+1$ and $^2l'-1$ terms can Auger decay. The fraction of the excited states that will not Auger decay is

$$(2l'+1)/[(2l'-1)+(2l'+1)+(2'l+3)]=\tfrac{1}{3}\ .$$

Thus for $l'=1$ and 2, I assumed $\frac{2}{3}$ of the excited-state terms would autoionize, while for $l'=0$ I assume all the excited-state terms autoionize providing it was energetically feasible. Chen and Crasemann[14] have shown that the Auger transition rate for $1s\ 2s^2 2p^2\ ^2P\rightarrow(1s^2 2s^2\ ^1S+$ continuum electron) is identically zero in *LS* coupling, and the above is merely a generalization of their result.

In the upper portion of Fig. 1 the PWBA calculations for C^{1+}-C^{3+} are shown as solid lines. The lower solid line is the calculation for direct ionization while the upper line is the sum of the cross section for direct ionization plus excitation followed by autoionization. The solid circles and triangles are Moore's Coulomb-Born calculations.[4,8] The open circles, triangles, and circles with error bars are experimental cross-section measurements. For C^{1+} the measured values are from Aitken *et al.*,[15] for C^{2+} from Woodruff *et al.*,[16] and for C^{3+} and C^{4+} from Crandall *et al.*[17]

For C^{1+} the PWBA and Coulomb-Born direct ionization calculations[4] are in excellent agreement from 36 eV to 2.4 keV. Near the cross-section peak, both direct ionization calculations are larger than experiment[15] by 10–15%. Near threshold, experiment is larger than the direct calculations. However, inclusion of excitation followed by autoionization makes the PWBA results slightly larger than experiment near threshold, increases the disagreement at the peak to 25%, but produces excellent agreement with experiment at 700 and 800 eV. Moores[18] has calculated the effect of excitation followed by autoionization over a limited energy range by a procedure different from that used here. At 30 eV his additional cross section is 2.1×10^{-17} cm^2, while my value is 1.35×10^{-17} cm^2. It is well known[19] that the cross section for electron excitation of positive ions is finite at threshold. Moores's[18] threshold value for C^+ is 0.86×10^{-17}, approximately the difference between

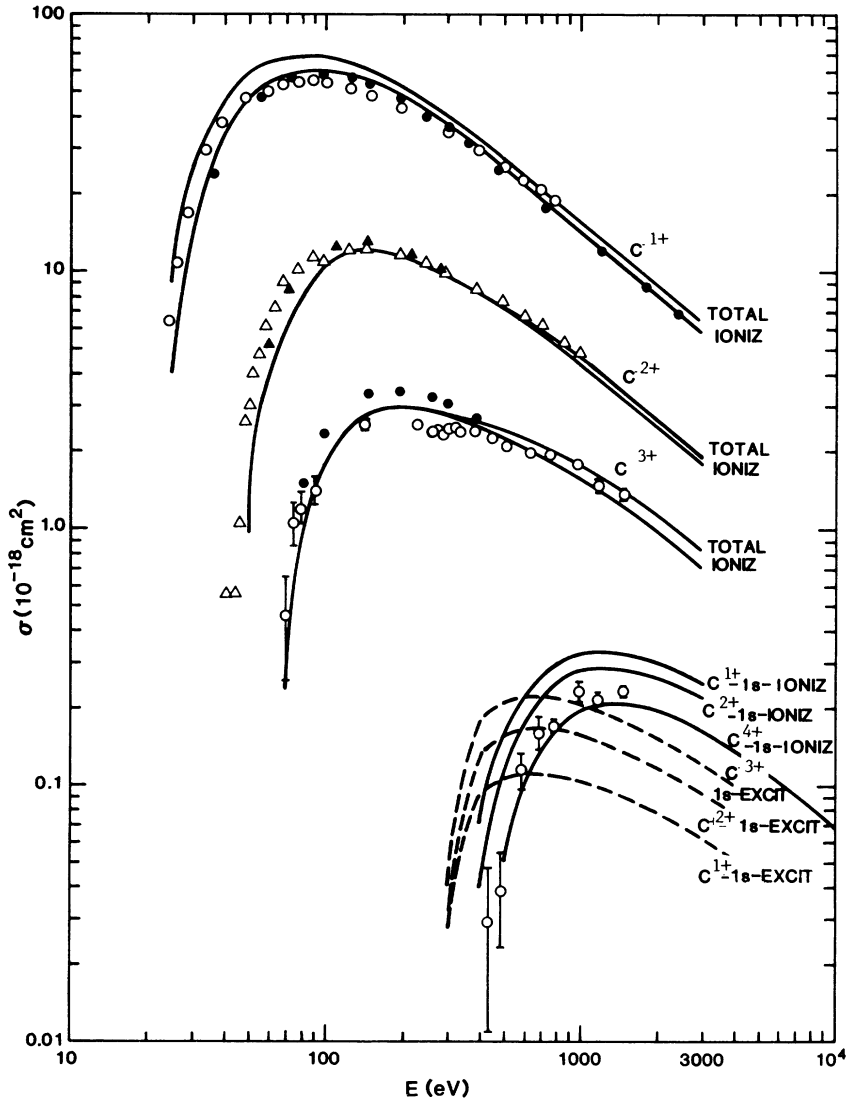

FIG. 1. Electron ionization cross section for carbon ions. The lower solid line is direct ionization. The upper solid line includes inner-shell excitation followed by autoionization. The solid circles and triangles are Coulomb-Born calculations from Refs. 4 and 8. The open circles and triangles are measurements from Ref. 15 (C^{1+}), Ref. 16 (C^{2+}), and Ref. 17 (C^{3+} and C^{4+}).

the two autoionization calculations at 30 eV. Thus the agreement between the C^{1+} experimental values and the PWBA total cross section near threshold is fortuitous.

For C^{2+}, the PWBA calculations are in excellent agreement with the measurements above 100 eV.[16] Above 100 eV, the PWBA calculations agree with the Coulomb-Born results[8] to better than 10%. Below 100 eV, the PWBA results underestimate the cross section significantly. For C^{3+}, the PWBA results are slightly lower (large error bars) than the measurements near threshold, are 20% higher at the peak, and in excellent agreement at high energy. The Coulomb-Born direct-ionization results are 15% higher than the PWBA results at the C^{3+} cross-section peak. Structure is seen in the experimental cross section between 240 and 350 eV. This could arise from a large threshold cross section for $1s^2 2s - 1s\,2s\,nl$ transitions. As mentioned above, the PWBA cannot address this question directly.

In the lower right-hand portion of Fig. 1 are shown the 1s ionization cross sections of C^{1+}, C^{2+}, and C^{4+} to show its variation with degree of ioni-

zation. Also shown is the calculated $1s$ total excitation cross section for C^{1+}, C^{2+}, and C^{3+}. As expected, it rises with degree of ionization. The peak in the C^{3+} $1s$ total excitation cross section is comparable to the size of the fluctuation in the measured C^{3+} ionization cross section between 240 and 350 eV, indirectly supporting the assignment of the fluctuations in the cross section to $1s$ excitation. The calculated C^{4+} ionization cross section is about 10% lower than the measured value.

To indicate the accuracy of the PWBA excitation cross section and, at the same time, its incorrect treatment of the threshold region, Fig. 2 compares the $1s^2\,2s\,^2S \rightarrow 1s\,2s^2\,^2S$ and $1s^2\,2s\,^2S \rightarrow 1s\,2s\,2p\,^2P$ PWBA excitation cross sections for C^{3+} with the six-state close-coupling calculations of Henry.[20] The PWBA $1s^2\,2s\,^2S \rightarrow 1s\,2s\,2p\,^2P$ cross section is compared with the sum of Henry's[20] $1s\,2s\,^3S\,2p$ and $1s\,2s\,^1S\,2p\,^2P$ cross sections. Above 440 eV, the PWBA calculations are within 10% of Henry's[20] results.

Figure 3 shows calculated and measured cross sections for N^{1+}, N^{2+}, and N^{3+}. For N^{1+} and N^{2+} the lower (upper) solid line is the calculated PWBA direct (total) cross section, the solid circles and triangles are Moores's Coulomb-Born calculations,[4,8] while the open circles and triangles are measurements on N^{1+} by Harrison *et al.*,[21] on N^{2+} by Aitken *et al.*,[15] and on N^{3+} by Crandall *et al.*[17] Shown as circles with slashes are the high-energy measurements of Donets and Ovsyannikov.[22] These data vary rapidly with energy in no comprehensible pattern. For N^{1+}, as for C^{1+}, the PWBA and Coulomb-Born direct ionization calculations are in excellent agreement, but overestimate the measured values by as much as 20%. Adding the contribution of excitation followed by autoionization increases the discrepancy. For N^{2+}, the measurements above 100 eV are closer to the PWBA direct than total cross section. Since the two PWBA cross sections differ by no more than 10%, this is excellent agreement. The Coulomb-Born calculations are also in excellent agreement above 100 eV. Below 100 eV, the Coulomb-Born direct calculations are higher than the PWBA direct calculations but agree with the PWBA total calculations. Experiment is as much as 25% higher than the PWBA total calculation. Moores[18] has calculated the autoionization contribution to the N^{2+} cross section. His total cross section is higher than the measurements. At 70 eV, Moores calculates an autoionization contribution 6.6×10^{-18} cm^2, whereas I find 3.0×10^{-18} cm^2. As mentioned in the discussion of C^{1+}, one expects the PWBA to underestimate the autoionization contribution near threshold.

For N^{3+}, the solid line is my direct ionization

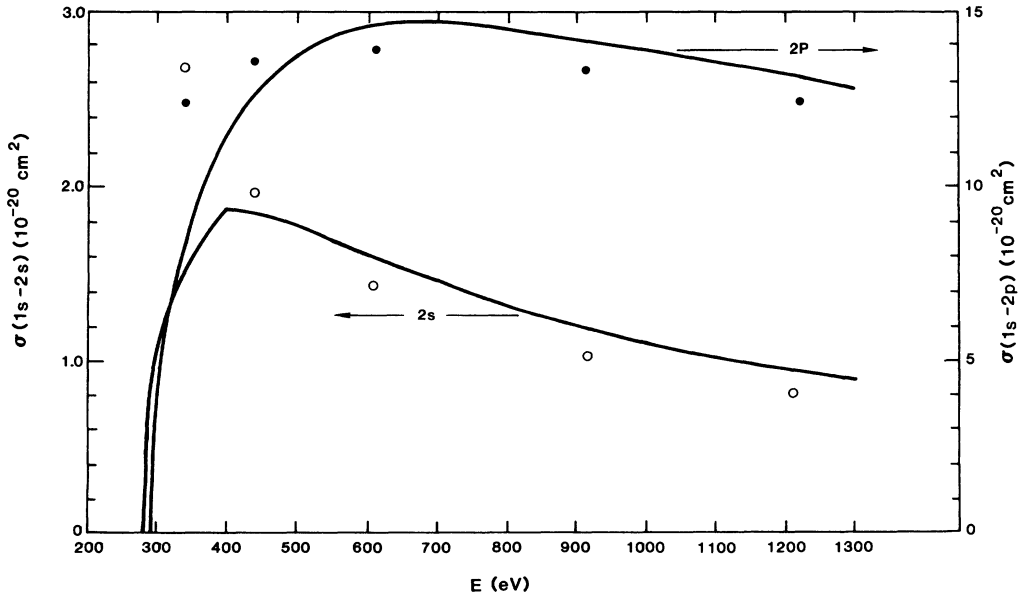

FIG. 2. Comparison of calculated (the results of this work) $1s^2\,2s\,^1\,^2S$-$1s\,2s^2\,^2S$ (lower) and $1s^2\,2s\,^1\,^2S$-$1s\,2s\,2p\,^2p$ (upper) excitation cross section in C^{3+} with the close-coupling (open and solid circles) calculation of Ref. 20. The discontinuity in slope at the peak of the $2s$ curve is an artifact of the energy grid used in the calculations.

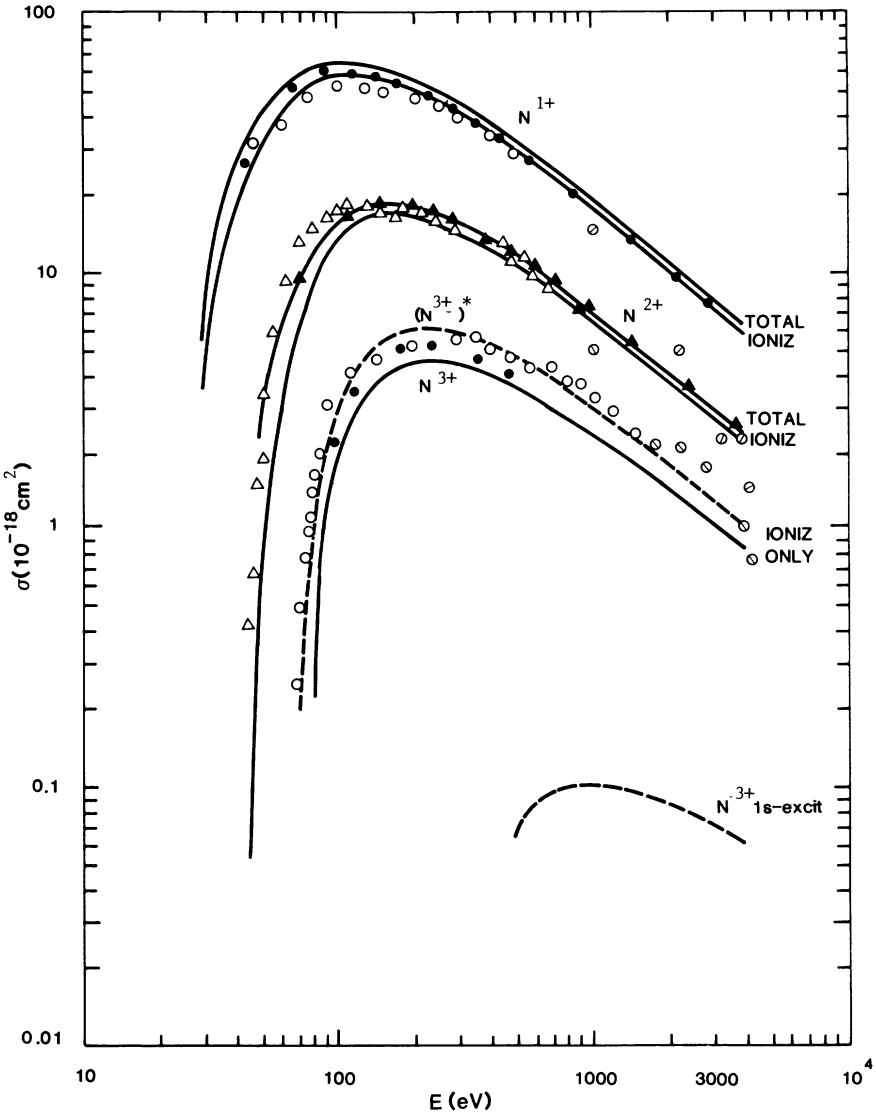

FIG. 3. Electron ionization cross section for nitrogen ions. The lower solid line is direct ionization. The upper solid line includes inner-shell excitation followed by autoionization. The solid circles and triangles are Coulomb-Born calculations of Refs. 4 and 8. The open circles and triangles are measurements from Ref. 21 (N^{1+}), Ref. 15 (N^{2+}), and Ref. 17 (N^{3+}). The circles with diagonals are from Ref. 22, southwest-northeast—N^{2+}, northwest—southeast N^{3+}.

calculation. It is as much as 30% below experiment. The Coulomb-Born results agree with experiment near the peak but approach the PWBA results at high energy. The dashed curve is the PWBA result for the metastable N^{3+} ion with the configuration $1s^2 2s^1 2p^1\,{}^3P$, calculated with orbitals for the $1s^2 2s^2$ central potential. The PWBA cross section for a beam with some metastable contamination would lie between these two curves. The lower right-hand corner shows the $1s$ total excitation cross section for N^{3+}. It would not significantly increase the total cross section. The peak $1s$ excitation cross section is 0.1×10^{-18} cm^2, comparable to the bump in the experimental data near 500 eV.

Figure 4 shows calculated and measured cross sections for O^{1+}, O^{2+}, O^{3+}, and O^{4+}. For the oxygen ions, the lower (upper) solid line is the calculated PWBA direct (total) cross section, the solid circles and triangles are Moores's Coulomb-Born results, while the open circles and triangles are measurements on O^{1+} and O^{2+} by Aitken and Harrison,[23] and O^{3+} and O^{4+} by Crandall *et al.*[17] The high-energy measurements of Donets and

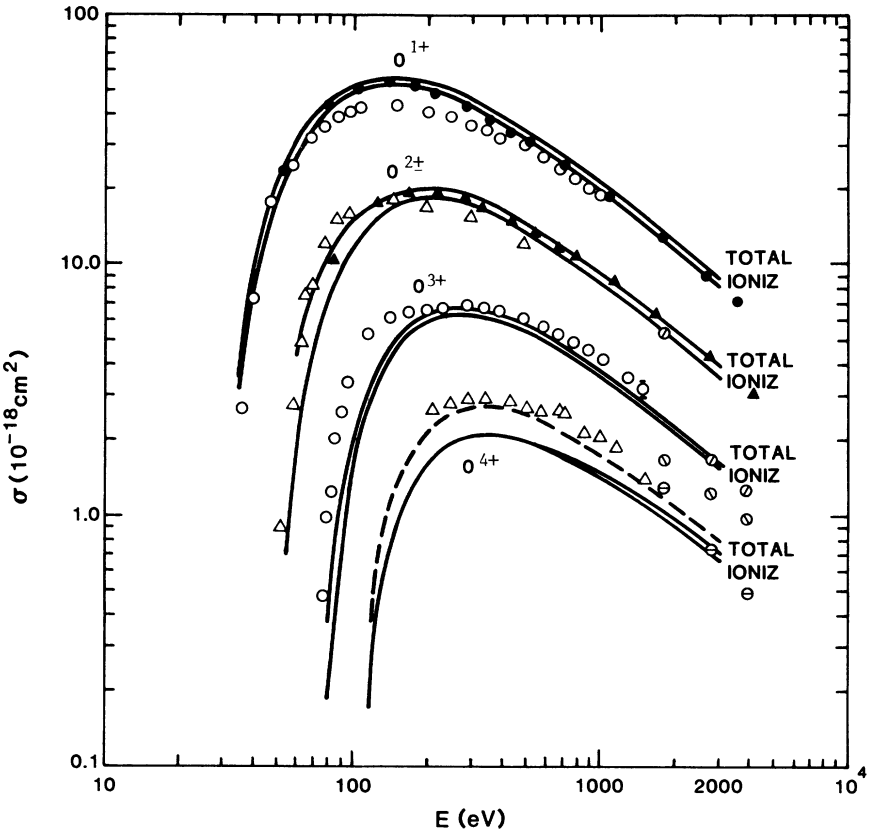

FIG. 4. Electron ionization cross section for oxygen ions. The lower solid line is direct ionization. The upper solid line includes inner-shell excitation followed by autoionization. The solid circles and triangles are Coulomb-Born calculations of Refs. 4 and 8. The open circles and triangles are measurements from Ref. 23 (O^{1+} and O^{2+}) and Ref. 17 (O^{3+} and O^{4+}). The circles with diagonals and bars are from Ref. 22, southwest-northeast diagonal—O^{2+}, southeast-northwest diagonal—O^{3+}, bar—O^{4+}.

Ovsyannikov[22] are also shown. For O^{1+}, as for C^{1+} and N^{1+}, the PWBA and the Coulomb-Born results are in excellent agreement above 100 eV, but 10—15% higher than the measurements at the peak of the cross section. For O^{2+} above 150 eV, the total and direct PWBA calculations are within 10% of each other. The Coulomb-Born direct cross section is above the PWBA direct cross section but below or equal to the total PWBA cross section. The experimental O^{2+} data are 10% below the PWBA direct results. For O^{3+}, above 200 eV experimental results are within 10% of the total PWBA results. Near threshold the PWBA total cross section for O^{3+} is significantly lower than the measurements. For O^{3+} the cross section for $2s$ excitation followed by autoionization is rapidly rising between 80 and 100 eV. It seems likely that the discrepancy in this energy range can be resolved by a treatment of excitation leading to finite cross sections at threshold. Stingl[5] has done a variety of CB calculations on O^{3+}, i.e., examining different choices of effective charge and the effect of exchange. At high energy Stingl's calculations neglecting exchange are in good agreement with the measurements, while the inclusion of exchange lowers the calculation by about 20%.

For O^{4+}, there is a significant discrepancy between the measurements and the ground-state PWBA calculations (solid curve). Crandall and Phaneuf[24] estimate that the metastable ($1s\,2s\,2p\,^4P$) contamination of their O^{4+} beam may be 50%. The dashed curve in Fig. 4 is the cross section for the metastable state calculated with orbitals for the $1s^2 2s^2$ central potential. It is 10—20% lower than the measurements. Thus the difference between these PWBA calculations for a mixture of ground-state and metastable ions and experiment would be greater than 10—20%.

The PWBA calculations presented here are in excellent agreement with the Coulomb-Born results

except near threshold. They are in good (25% or better) agreement with the measurements except near threshold, and except for N^{3+} and O^{4+}.

III. SCALED CROSS SECTIONS AND SOME CORRECTIONS

In Fig. 5, the solid lines are direct and total ionization cross sections for fluorine ions, calculated explicitly. The dashed lines are obtained from the scaling laws given in Ref. 7. The scaled cross sections are lower than the explicit calculations, with the difference ranging from 30% for F^{1+} to 10% for F^{4+} and F^{5+}. Similar differences with the scaling procedure occur for the ions treated in Sec. II. This section examines the causes of the differences and corrections for improving the scaled cross sections using a smaller set of calculations than the GOS.

The scaling hypothesis advanced in Ref. 7 is that subshell ionization cross section can be described by

$$(E_{nl})^{\alpha}\sigma(E,E_{nl})=f_{nl}(E/E_{nl})=f_{nl}(\eta)\ ,$$

where E_{nl} is the subshell ionization energy, E is the incident electron energy, $f_{nl}(\eta)$ is a shape function that does not change significantly over wide ranges of E_{nl}, and α is a parameter determined by explicit calculations. For E_{nl} very large, $\alpha=2$, defining

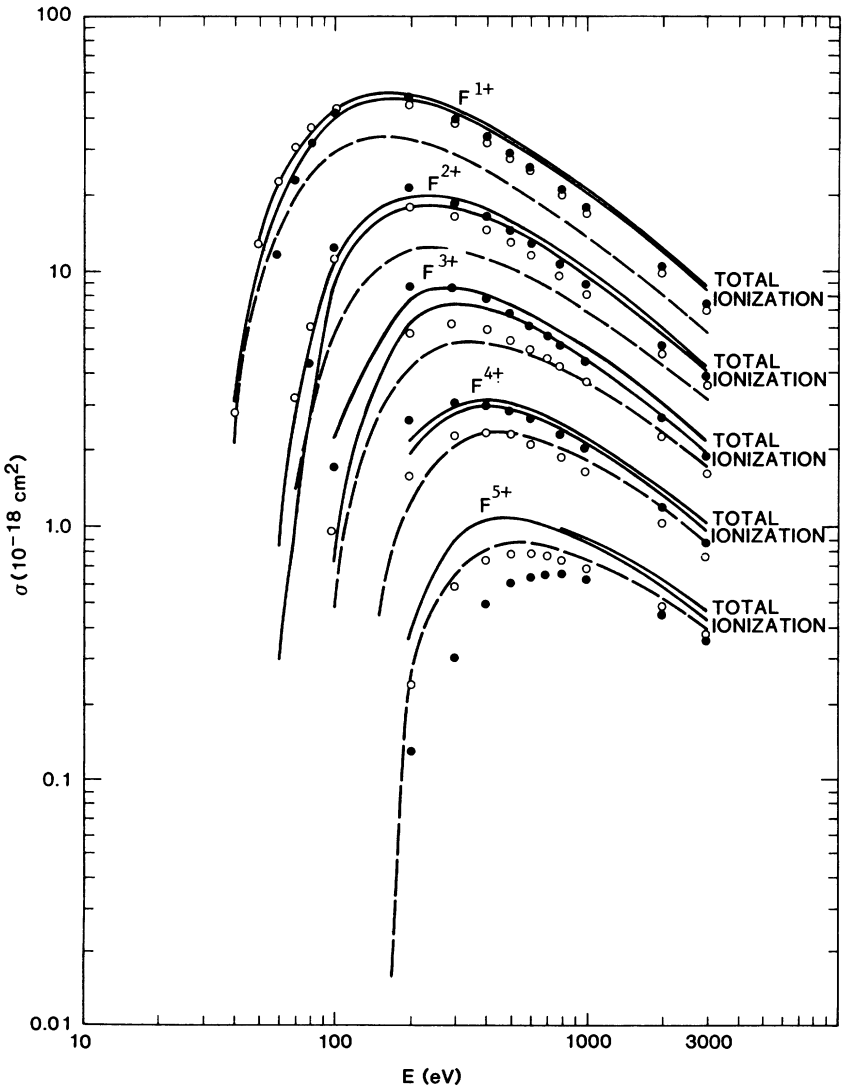

FIG. 5. Electron ionization cross section for fluorine ions. The lower solid line is direct ionization. The upper solid line includes inner-shell excitation followed by autoionization. The dashed curves are direct ionization results using the scaling procedure in Ref. 7. The solid (open) circles are corrected scaled cross sections using Eqs. (3a) and (3b).

the region of classical scaling. I determine α by plotting peak subshell cross section times subshell ionization energy squared versus subshell ionization energy. In Fig. 6 such a plot is shown for the $2s$ and $2p$ subshells. The solid lines connect neutral atom values. Values for C, O, and F ions are also shown. The ion values approach the classical limit more rapidly with increasing E_{nl} than do the neutral atom values. This occurs, in part, because the ground-state orbital approaches the hydrogenic value and the classical limit is the hydrogenic limit. Figure 6 shows for Ne, O^{1+}, and C^{2+} that even though the $2s$ ionization energies (3.35 Ry) are almost equal, the peak cross sections differ significantly. In Fig. 7 the $2s$ orbitals for these ions are shown and compared with a hydrogenic orbital with $z^* = 2\sqrt{3.35}$. The orbitals move outward with increasing degree of ionization even though the potential at large distances becomes more attractive with increasing degree of ionization. This is less effective than the decrease in the attractive potential at small distances.

After choosing α_{nl}, the second step in the scaling hypothesis is to choose the shape function $f_{nl}(E/E_{nl})$ from the calculated cross section for a representative element. For these ions the ionization energy range is the rising portion of the curves in Fig. 6. In scaling the $2s$ and $2p$ cross sections, the argon values were chosen as the representative elements because of the availability of experimental data for comparison. To gauge the error in this choice, I show in Fig. 8 the scaled argon cross sections as a solid line and scaled cross sections for Na, Mg, Al, Si, and S as points. Except for the $2p$ cross section of Na and Mg at low E/E_{2p}, all the scaled cross sections agree to 20% or better. Asymptotically, the cross section for the elements shown as points are $10-10\%$ larger than the scaled argon cross sections. This is the cause of some of the differences between scaled and explicitly calculated cross sections in Fig. 5. However, it cannot account for the difference at the peak of the cross section.

An interesting feature of the calculations shown in Fig. 8 is the small variation in scaled cross section in the asymptotic region. Here one expects the cross section to be dominated by an integral over the optical oscillator strength, and there is no inherent reason to expect the ionization energy scaling parameter α_{nl}, chosen at the cross-section peak, to accurately predict scaling in the asymptotic region.

The third step in the scaling hypothesis is the assertion that the scaled cross sections obtained from neutral atom calculations can be extended to ions. A sufficient condition for this to be valid is the equality of the subshell generalized oscillator strengths for ions and atoms with equal subshell ionization energy. In Fig. 9 the $2p$ GOS for Na ($E_{2p}=2.54$ Ry) is compared with the $2p$ GOS for F^{1+} ($E_{2p}=2.55$ Ry), multiplied by $\frac{3}{2}$ to scale the latter to a full shell. In Fig. 10 a similar comparison is made for the $2p$ GOS of Si ($E_{2p}=8.23$ Ry) and F^{4+} ($E_{2p}=8.01$ Ry). In both cases the scaled

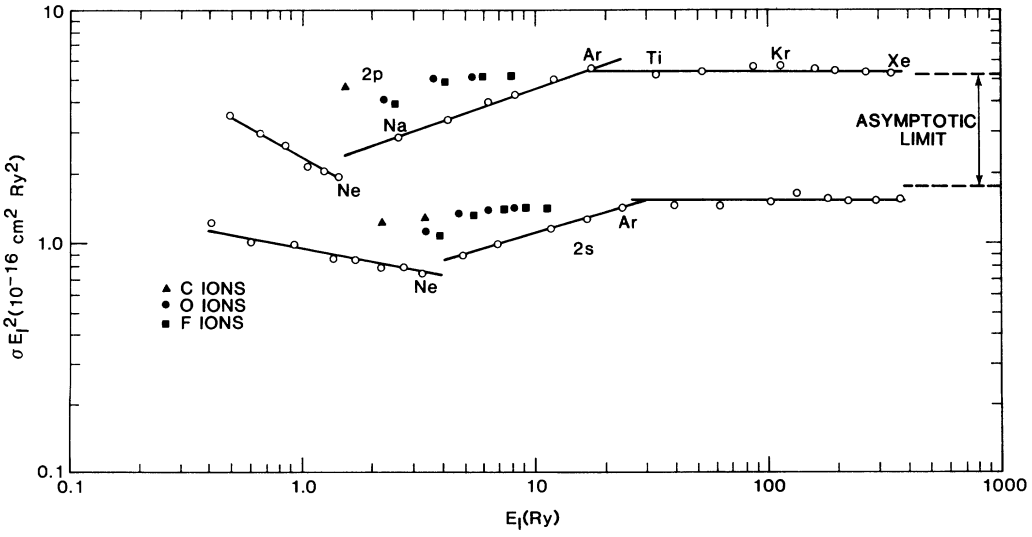

FIG. 6. Peak subshell cross section times subshell ionization squared versus subshell ionization energy for the $2s$ and $2p$ subshells. The solid lines are obtained from neutral atom calculations. The points are for C, O, and F ions.

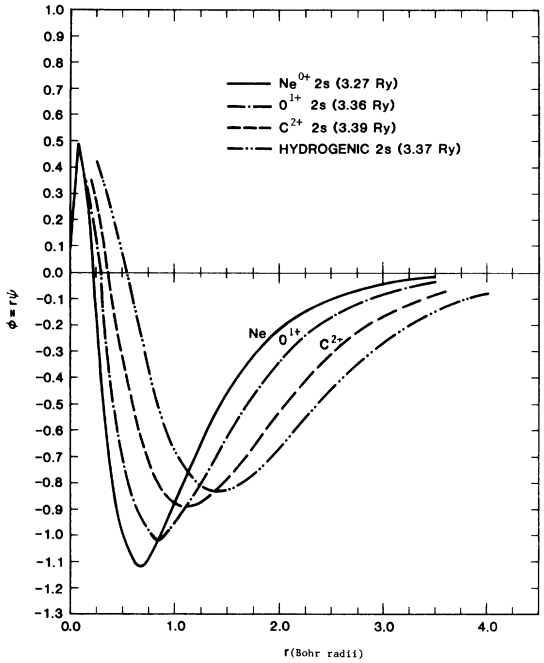

FIG. 7. Comparison of the isoenergetic $2s$ orbitals of Ne, O^{1+}, C^{2+}, and a hydrogenic orbital.

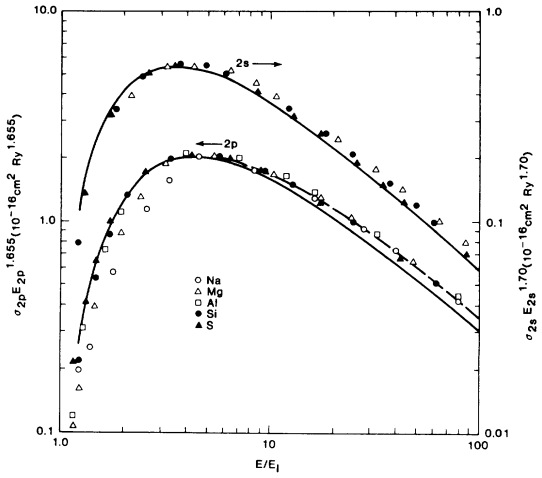

FIG. 8. Calculated $2s$ and $2p$ electron ionization cross sections of Na, Mg, A, Si, and S (points) and Ar (solid curve) in scaled form.

variables $\epsilon=\epsilon/E_{2p}$ and K^2/E_{2p} are used. In both cases for $K^2/E_{2p}\geq 1$ and for ϵ/E_{2p} up to 3, the GOS values are comparable. Near the Bethe ridge ($\epsilon=K^2$) the GOS for $\epsilon/E_{2p}=10$ and 25 are comparable, but away from the Bethe ridge the ionic GOS at $\epsilon/E_{2p}=10$ and 25 are considerably lower than the atomic values. This merely reflects the orbital expansion such as that in Fig. 7, and the insensitivity of high-energy continuum orbitals to the difference in potentials. For $K^2/E_{2p}\leq 1$ the GOS are quite different and suggest that one can use this difference to generate a correction to the scaled cross sections, as was done in Ref. 9. Assuming for $K^2/E_{2p}\geq 1$, that the atom and ion GOS are equal one can rewrite Eq. (1) as

$$\sigma_{nl}(E,E_{nl},\text{ion})=\sigma_{nl}(E,E_{nl},\text{atom})+\frac{4\pi a_0^2}{E}\int_0^{E_u}\frac{d\epsilon}{\epsilon+E_{nl}}\int_{K^2_{\min}}^{E_{nl}}\frac{dK^2}{K^2}\Delta(K^2,\epsilon)\,, \tag{2}$$

where

$$\Delta(K^2,\epsilon)=\frac{df_{nl}}{d\epsilon}(\epsilon,K^2)\bigg|_{\text{ion}}-\frac{df_{nl}}{d\epsilon}(\epsilon,K^2)\bigg|_{\text{atom}}\,,$$

and E_u is the smaller of $(E-E_{nl})/2$ or $\sqrt{4EE_{nl}}-2E_{nl}$. The atomic GOS is for a pseudoatom with the same subshell ionization energy as the ion. With the above assumption, this is an exact expression. One would like to replace $\Delta(K^2,\epsilon)$ with the difference in optical GOS. However, Figs. 9 and 10 suggest that the slope of GOS near $K^2=0$ is important. Thus, we approximate $\Delta(K^2,\epsilon)$ by either

$$\Delta(K^2,\epsilon)=\Delta(0,\epsilon)+\frac{d}{dK^2}\Delta(K^2,\epsilon)\bigg|_{K^2=0}K^2\,, \tag{3a}$$

or

$$\Delta(K^2,\epsilon)=\Delta(0,\epsilon)+\frac{d}{dk^2}\Delta(K^2,\epsilon)\bigg|_{K^2=0}K^2-\left[\Delta(0,\epsilon)+\frac{d}{dK^2}\Delta(K^2,\epsilon)\bigg|_{K^2=0}E_{nl}\right]\frac{K^4}{E_{nl^2}}\,. \tag{3b}$$

In case (3b) a term quadratic in K^2 is included with the additional constraint $\Delta(E_{nl},\epsilon)=0$. This is consistent with the assumption that the GOS are equal for $K^2/E_{nl}\geq 1$. If the difference in GOS near $K^2/E_{nl}=1$ is small, then the two corrections should be comparable, indicating the $K^2/E_{nl}\approx 0$ region is dominating the correction. Then the difference in GOS due to the difference in atomic potentials is ade-

quately reflected in the difference in the photoionization cross section. If the difference in GOS near $K^2/E_{nl}=1$ is not small, but the quadratic term in K^2 is not dominant then the two corrections in conjunction with the scaled cross sections should establish bounds. If the quadratic term in the expansion of the difference in GOS is large and the difference in GOS near $K^2/E_{nl}=1$ is large then the corrections are not useful and explicit calculations must be done.

Up to a structure factor (C) the GOS is given by

$$\frac{df}{d\epsilon}(\epsilon,K^2)=\frac{C(\epsilon+E_{nl})}{K^2}\sum_{l't}(2l'+1)(2t+1)\begin{bmatrix} l & l' & t \\ 0 & 0 & 0 \end{bmatrix}^2\left|\int_0^\infty \phi nl\phi\epsilon l' j_t(Kr)d\vec{r}\right|^2 \tag{4a}$$

so that

$$\frac{df}{d\epsilon}(\epsilon,0)=C(\epsilon+E_{nl})\tfrac{1}{3}\sum_{l'}(2l'+1)\begin{bmatrix} l & l' & 1 \\ 0 & 0 & 0 \end{bmatrix}^2\left|\int_0^\infty \phi nl\phi\epsilon l' r\,d\vec{r}\right|^2 \tag{4b}$$

and

$$\left.\frac{d^2f}{d\epsilon\,dK^2}\right|_{K^2=0}=C(\epsilon+E_{nl})\tfrac{1}{30}\sum(2l'+1)\left[-\begin{bmatrix} l & l' & 1 \\ 0 & 0 & 0 \end{bmatrix}^2\left|\int_0^\infty \phi n\epsilon\phi\epsilon l' r\,d\vec{r}\int_0^\infty \phi nl\phi\epsilon l' r^3 d\vec{r}\right|\right.$$
$$\left.+\frac{1}{6}\begin{bmatrix} l & l' & 2 \\ 0 & 0 & 0 \end{bmatrix}^2\left|\int_0^\infty \phi nl\phi\epsilon l' r^2 d\vec{r}\right|^2\right], \tag{4c}$$

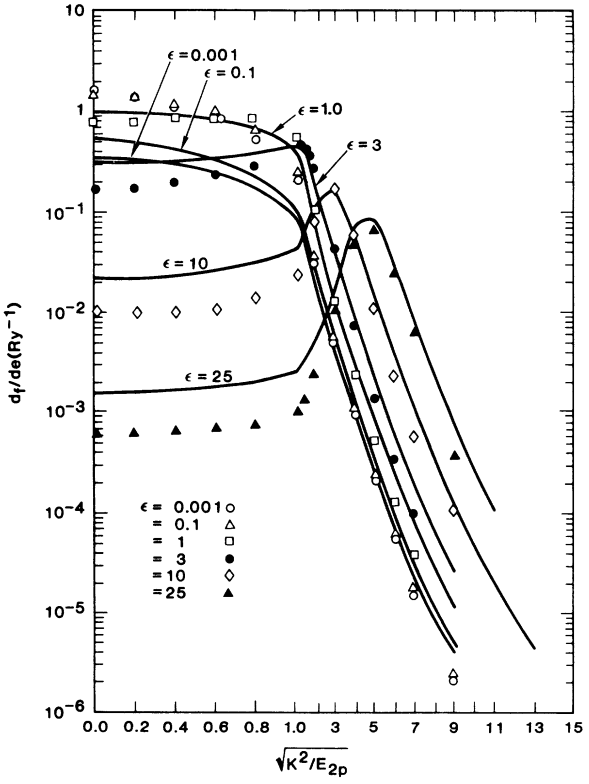

FIG. 9. Comparison of the Na ($E_I=2.54$ Ry) and F^{1+} ($E_I=2.55$ Ry) $2p$ GOS as a function of scaled momentum transfer with scaled secondary electron energy as parameter. The solid lines are the neutral atom values.

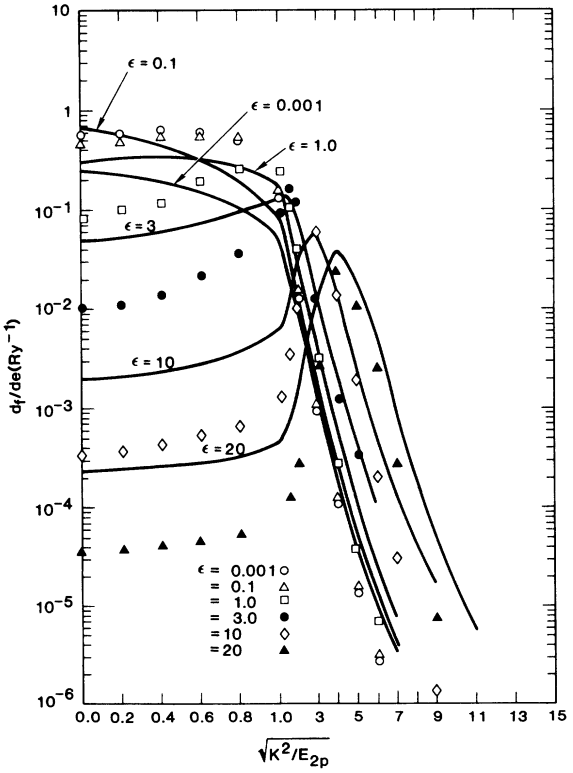

FIG. 10. Comparison of the Si ($E_I=8.25$ Ry) and F^{4+} ($E_I=8.01$ Ry) $2p$ GOS as a function of scaled momentum transfer with scaled secondary electron energy as parameter. The solid lines are the neutral atom values.

i.e., one can obtain the correction by calculating matrix elements of r^2 and r^3, as well as r.

In evaluating the corrections the explicitly calculated GOS were used to determine $d\Delta(K^2,\epsilon)/dK^2$. The ion subshell eigenvalues and those of the pseudoatoms are listed in Table I. The scaled cross sections plus corrections are shown as solid [using Eq. (3a)] and open [using Eq. (3b)] circles in Fig. 5.

For F^{1+} and F^{2+} the scaled cross sections with corrections agree with the explicitly calculated cross section at the peak, and are 10—15 % lower at high energies. This is consistent with the error introduced in using the scaled argon cross sections in place of the pseudoatoms. For F^{3+} and F^{4+} the corrections bound the explicitly calculated cross section when the high-energy error in scaling was taken into account.

For F^{5+} the corrections fail. In Fig. 11 the $2s$ GOS for Si ($E_{2s}=11.84$ Ry) and F^{5+} ($E_{2s}=11.35$ Ry) are shown. For $\epsilon/E_{2s}=0.001$ and 0.1 the difference in GOS is large at $K^2/E_{2s}=1$, and a two-term expansion of the GOS poorly reproduces the rise in the F^{5+} at GOS at $(K^2/E_{2s})^{1/2}=0.6$ and 0.8.

On the other hand, for F^{5+} the cross section calculated explicitly is never more than 20% larger than the scaled cross section. Figure 6 indicates that, in general, subshell ionization cross sections approach the classical limit more rapidly with ionization energy than do neutral atoms. Then the correction to the scaled cross section is likely to be valid if the correction moves the scaled cross section toward the classical limit. If the correction moves the scaled cross section away from the classical limit, then neglected features of the GOS are likely to be important and the correction should be neglected.

TABLE I. Ionization energies of $2s$ and $2p$ subshells of fluorine ions and associated pseudoatoms.

F^{n+}			Pseudoatoms	
n	Subshell	E_{nl}(Ry)	E_{nl}	Z
1	$2s$	3.91	3.24/4.84	Ne/Na
	$2p$	2.55	2.54	Na
2	$2s$	5.52	4.84	Na
	$2p$	4.18	4.22	Mg
3	$2s$	7.32	6.88	Mg
	$2p$	6.00	6.38	Al
4	$2s$	9.25	9.40	Al
	$2p$	8.01	8.25	Si
5	$2s$	11.35	11.84	Si

IV. CONCLUSIONS

The utility of the PWBA vis-á-vis the Coulomb-Born or distorted-wave approximations lies in its relative simplicity; the Bethe integral explicitly removes one integral over spatial coordinates. The surprising result of these PWBA calculations is the excellent agreement with the Coulomb-Born results, except, as expected, near threshold. The scaling hypothesis is an attempt to further simplify the estimation of electron ionization cross sections, and is accurate to better than a factor of 2. The scaling hypothesis can be improved by a correction [Eq. (2)] using ionic GOS calculated over a narrow range of momentum

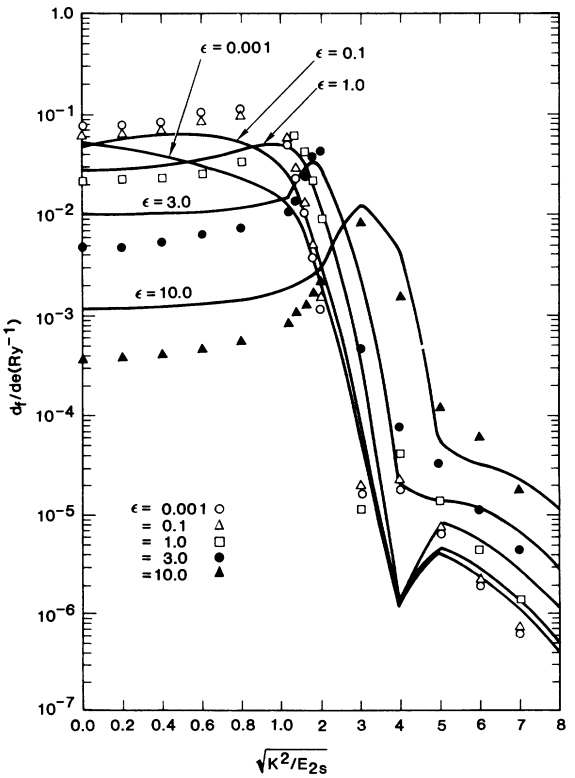

FIG. 11. Comparison of the Si ($E_I=11.84$ Ry) and F^{5+} ($E_I=11.35$ Ry) $2s$ GOS as a function of scaled momentum transfer with scaled secondary electron energy as parameter. The solid lines are neutral atom values.

transfer and secondary electron energy, i.e., $K^2/E_{nl} \leq 1$ and $\epsilon/E_{nl} \leq 1$. This leads to a significant saving in computer time over full range GOS calculations. A simpler, if less accurate, correction to the scaling hypothesis can be made using the optical oscillator strength and its momentum-transfer derivative, as shown in Sec. III.

This work was supported by the U.S. Department of Energy.

[1]W. Lotz, Z. Phys. 216, 241 (1968).
[2]A. Burgess, H. P. Summers, D. M. Cochrane, and R. P. W. McWhirter, Mon. Not. R. Astron. Soc. 179, 275 (1977).
[3]L. B. Golden and D. H. Sampson, J. Phys. B 10, 2229 (1977).
[4]D. L. Moores, J. Phys. B 5, 286 (1972).
[5]E. Stingl, J. Phys. B 5, 1160 (1972).
[6]S. M. Younger, Phys. Rev. A 22, 111 (1980); A 22, 1425 (1980).
[7]E. J. McGuire, Phys. Rev. A 16, 73 (1977).
[8]D. L. Moores, J. Phys. B 11, L403 (1978).
[9]E. J. McGuire, Phys. Rev. A (in press).
[10]Dr. S. M. Younger has kindly pointed out that in Phys. Rev. A 3, 267 (1971) and A 16, 62 (1977) I used $\epsilon_{max}=E_0/2$. This was a misprint rather than a calculational error as $\epsilon_{max}=(E_0-E_{nl})/2$ was always used in the computer program.
[11]Most recently in E. J. McGuire, Phys. Rev. A 22, 868 (1980).
[12]F. Herman and S. Skillman, *Atomic Structure Calculations* (Prentice-Hall, Englewood Cliffs, N.J., 1963).
[13]C. E. Moore, *Atomic Energy Levels*, National Bureau of Standards (U.S.) Circ. No. 467 (U.S. GPO, Washington, D.C., 1957).
[15]K. L. Aitken, M. F. A. Harrison, and R. D. Rundle, J. Phys. B 4, 1189 (1971).
[16]P. R. Woodruff, M-C. Hublet, M. F. A. Harrison, and E. Brook, J. Phys. B 11, L679 (1978).
[17]D. H. Crandall, R. A. Phaneuf, and D. C. Gregory, Oak Ridge National Laboratory Report No. ORNLITM-7020, 1979 (unpublished).
[18]D. L. Moores, J. Phys. B 12, 4171 (1979).
[19]M. J. Seaton, in *Atomic and Molecular Processes*, edited by D. R. Bates (Academic, New York, 1962).
[20]R. J. W. Henry, J. Phys. B 12, L309 (1979).
[21]M. F. A. Harrison, K. T. Dolder, and P. C. Thonemann, Proc. Phys. Soc. London 82, 368 (1963).
[22]E. D. Donets and V. P. Ovsyannikov, Report No. P7-10780, Joint Institute of Nuclear Research, Dubna (English Translation available from ORNL-tr-4616, Tech. Inform. Center, P.O. Box 62, Oak Ridge, Tennessee).
[23]K. L. Aitken and M. F. A. Harrison, J. Phys. B 4, 1176 (1971).
[24]D. H. Crandall and R. A. Phaneuf, in *Abstracts of Contributed Papers, XI International Conference on the Physics of Electronic and Atomic Collisions, Kyoto, Japan, 1979*, edited by N. Oda and K. Takayanagi (North-Holland, Amsterdam, 1980).